

pubs.acs.org/JPCB Article

# Azide Anion Interactions with Imidazole and 1-Methylimidazole in **Dimethyl Sulfoxide**

Debkumar Rana,\* Anna Luisa Upterworth, Marc-Oliver Winghart, Daniel Sebastiani,\* and Erik T. J. Nibbering\*



Cite This: J. Phys. Chem. B 2025, 129, 8192-8200



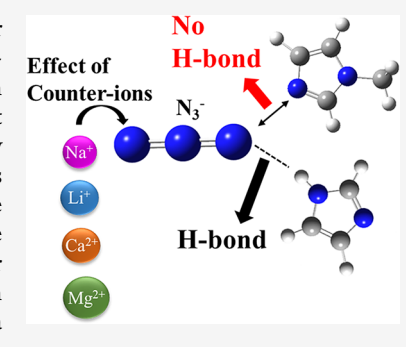
**ACCESS** I

III Metrics & More

Article Recommendations

Supporting Information

ABSTRACT: We chose imidazole (HIm) and 1-methylimidazole (1-MeIm) to probe their interaction with the azide anion. In dimethyl sulfoxide (DMSO), the formation of hydrogenbonded pairs between the azide ion and HIm is clearly distinguishable from free azide ions in FT-IR spectra, allowing for accurate spectra differentiation. HIm can both donate and accept hydrogen bonds, forming hydrogen-bonded networks, while 1-MeIm can accept only hydrogen bonds, preventing hydrogen-bonded network formation. To differentiate the roles of hydrogen and nonhydrogen bonding interactions with azide at ultrafast time scales, we use femtosecond mid-IR pump-probe spectroscopy. From the time-resolved data analysis, we observe a clear difference in vibrational population relaxation times of the azide anion under the presence of HIm or 1-MeIm. With the addition of HIm, the vibrational population relaxation time of the azide anions decreases by a factor of 1.6 to 1.7, which we attribute to a more efficient energy dissipation pathway provided through the strong hydrogen bonds



between the azide anion and HIm. Furthermore, we investigated the influence of alkali and alkaline earth metal counterions on the vibrational relaxation of azide ion pairs and found a dependence on the charge and size of the counterions. An assessment of the molecular distribution function from molecular dynamics simulation supports our results on the interactions between different ion species.

### 1. INTRODUCTION

Ion speciation plays a crucial role in solution chemistry and biology. Different ionic species participate in reactions with their own characteristic features and this results in a specific dynamical equilibrium. Under dynamical equilibrium, among different ion-solvent configurations, oppositely charged ions can associate to form various ion pairs, and the reverse processes also occur with new formations of solvation shells around them. Such ion pairing dynamics are of fundamental importance in determining the properties of electrolyte solutions as well as understanding chemical and biological processes in electrolyte solutions. 1,2 Ions also play an important role in determining the 3D structure of proteins in aqueous solutions by either directly interacting with proteins or changing the properties of bulk water.<sup>3,4</sup> Such a list of ions that are capable of stabilizing or destabilizing protein structures in electrolyte solutions has been known as the Hofmeister series. 5,6 To study complex or ion pair formation in electrolyte solutions, a variety of experimental methods, such as conductometry, dielectric relaxation spectroscopy, ultrasonic relaxation, temperature-jump relaxation, and other spectroscopic methods, 11 have been used. Dielectric and ultrasonic relaxation spectroscopic methods are effective for studying the dynamic properties of electrolyte solutions, providing information on the rotational time scales of dipolar species such as contact ion pairs (CIPs), solvent-separated ion pairs

(SIPs), and doubly solvent-separated ion pairs (2SIPs). 12 The components from these ion pair configurations have, however, a significant spectral overlap in their dielectric or ultrasonic response, thus resulting in ambiguities in the assignment due to the dynamics of rotation and dissociation of different ion pairs. 12,13 These experimental methods are frequency-domain techniques, so they have a limitation in resolving ion pairing dynamics occurring on picosecond time scales. In addition to these experimental efforts, ion pairing dynamics have also been extensively investigated by the use of molecular dynamics (MD) simulations, which provided information on the potential of mean forces as well as on ion pair associationdissociation processes.<sup>14</sup> In addition to frequency-domain IR spectroscopy and molecular dynamics simulations, timeresolved infrared spectroscopy has been successfully employed to investigate ultrafast solvation and ion dynamics in electrolyte solutions. Ghosh et al. 15 have used anionic probes to capture transient interactions and solvation shell fluctuations with a subpicosecond resolution. The effect of contact ion pairs

Received: March 26, 2025 Revised: July 23, 2025 Accepted: July 25, 2025 Published: August 4, 2025





on determining the electric conductivity of liquid electrolytes and ionic aqueous solutions and in the stabilization of DNA and RNA structures is studied largely using time-resolved infrared spectroscopy. <sup>16</sup> In parallel, femtosecond two-dimensional infrared spectroscopy in conjunction with density functional theory has allowed for a dynamic characterization of contact ion pairs with different counterions. <sup>17</sup>

Herein, we investigate contact ion pairing using linear and ultrafast mid-infrared pump-probe spectroscopy in combination with MD simulations. We choose the azide  $(N_3^-)$  anion as a vibrational probe due to its high molar extinction coefficient and its frequency sensitivity to local environments. <sup>18</sup> The N<sub>3</sub> ion exhibits a strong infrared-active asymmetric stretching band within the 2000-2100 cm<sup>-1</sup> spectral range. This characteristic makes it particularly useful for identifying ion pairs, higher-order aggregates, and various intermolecular interactions such as hydrogen bonding and ion-dipole interactions. Numerous experimental studies have investigated the spectroscopy and dynamics of the antisymmetric stretching vibrational mode of the azide anion in different environments, including the gas phase, <sup>19</sup> bulk solvents, <sup>20,21</sup> reverse micelles, <sup>22,23</sup> and biological systems. <sup>24</sup> Previously, it has been reported that the N<sub>3</sub><sup>-</sup> anion forms ion pairs with alkali metals and alkaline earth metals in polar solvents.<sup>11</sup> The infraredactive mode within the 2000-2100 cm<sup>-1</sup> range of the N<sub>3</sub><sup>-</sup> ion is sensitive to the interaction with metal and alkaline earth metal ions, which can be clearly observed by inspection of its frequency shift.  $^{25}$  The vibrational lifetime of the  $N_{3}^{\,-}$  anion in the presence of alkali and alkaline earth metal cations in polar or apolar solvents is well reported.  $^{26}$  This makes the  $N_3^-$  ion highly versatile in the investigation of the formation of contact pairs, also with a large variety of organic molecules.<sup>27</sup> We have chosen imidazole (HIm) and 1-methylimidazole (1-MeIm), two simple organic molecules that contain a five-membered heterocyclic ring with two N atoms at the 1 and 3 positions, to understand the contact pair interactions with the  $N_3^-$  ion. HIm is a functional group of the amino acid histidine which participates in proton transfer processes. 28,29 The proton conductivity of the HIm molecule is as high as water, as it can form hydrogen-bonded networks.<sup>30</sup> HIm acts as a hydrogen bond donor and acceptor due to its two nitrogen atoms, one with and one without the H atom; in contrast, 1-MeIm cannot donate a hydrogen bond. The structures of (a) HIm and (b) 1-MeIm and the schematic interaction between (c)  $N_3^-$  and (d) HIm are shown in Figure 1. Previously, Shin et al.<sup>31</sup> have investigated the hydrogen and nonhydrogen bonding liquid dynamics of HIm and 1-MeIm by probing the selenocyanate (SeCN) anion using time-resolved infrared spectroscopy and MD simulation. In their study, they have taken pure HIm and 1-MeIm in the liquid phase at 95 °C. In our study, we have selected dimethyl sulfoxide (DMSO) as the solvent, wherein the solvent separates and contact ion pairs of the azide anion can be found. DMSO is an interesting polar solvent as S=O describes the strength of the surrounding electric fields and the hydrogen bonding status.<sup>32-34</sup> For a more profound understanding of the hydrogen bonding interaction of HIm with solvent-separated and contact ion pair azides, it is important to systematically explore a wider range of mono- and divalent ions. We have chosen alkali and alkaline earth metals (Na+, Li+, Ca<sup>2+</sup>, Mg<sup>2+</sup>), which form solvent-separated and contact ion pair species with  $N_3^-$  ions in DMSO. In addition to the experiments, classical molecular dynamics simulations are performed to reveal the distinct differences between the

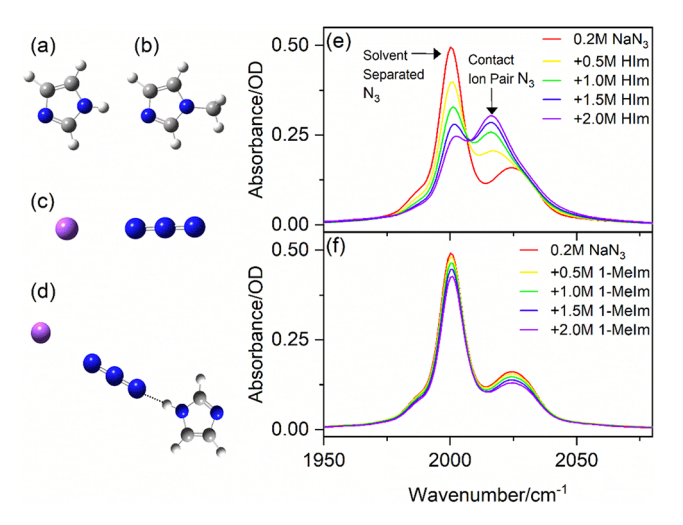


Figure 1. Left panel: ball-and-stick models of (a) imidazole (HIm), (b) 1-methylimidazole (1-MeIm), (c) sodium azide (NaN $_3$ ), and (d) NaN $_3$  interacting with HIm. Right panel: FT-IR spectra of the asymmetric stretching mode of sodium azide (NaN $_3$ ) with different concentrations of (e) HIm and (f) 1-MeIm in DMSO.

contact geometries ensuing the interactions and to provide a systematic and quantitative picture of ion pairs and contact pairs containing the azide anion.

#### 2. METHODS

2.1. Sample Preparation. Imidazole (HIm) (purity >99%), 1-methylimidazole (1-MeIm) (>99%), sodium azide (NaN<sub>3</sub>), tetrabutylammonium azide (TBA-N<sub>3</sub>), and metal halides (LiCl, CaCl2, and MgCl2) were all purchased from Sigma-Aldrich. The 0.20 M N<sub>3</sub><sup>-</sup> solution was prepared by dissolving TBA-N<sub>3</sub> in dimethyl sulfoxide (DMSO). In DMSO, TBA-N<sub>3</sub> is fully dissociated into tetrabutylammonium (TBA<sup>+</sup>) and N<sub>3</sub><sup>-</sup> ions. Furthermore, to prepare the ion pairs, TBA-N<sub>3</sub> and halide salts were dissolved in DMSO where the concentration of TBA-N3 is 0.20 M and the concentrations of halide salts ([LiCl] = 0.55 M, [CaCl<sub>2</sub>] = 0.30 M, [MgCl<sub>2</sub>] = 0.30 M) were varied such that the IR absorbance of the contact ion pairs was about 0.3-0.4 OD. Since the solubility of LiCl and MgCl<sub>2</sub> salts is relatively low in DMSO, we needed to use a heat bath to fully dissolve the sample. In the case of NaN<sub>3</sub>, we have dissolved 0.20 M NaN3 directly into DMSO.

**2.2. FT-IR Measurements.** Linear infrared absorption spectra were recorded with a Fourier transform infrared (FT-IR) spectrometer (Bruker Vertex 80) with a 1 cm $^{-1}$  spectral resolution. The samples were held in a commercial liquid cell (Harrick) in between two 1 mm thick CaF $_2$  windows separated by a 12  $\mu m$  Teflon spacer.

**2.3.** Mid-IR Pump—Probe Spectroscopy Setup. Timeresolved experiments were carried out using a home-built mid-IR pump—probe setup. The details of the experimental setup are shown in Figure S1. Pump and probe beams were centered at 5  $\mu$ m and kept in parallel polarization. All of the pump—probe measurements were performed with the samples held in a commercial liquid cell (Harrick) between two 1 mm thick CaF<sub>2</sub> windows separated by a 12  $\mu$ m Teflon spacer.

**2.4.** Computational Details: Molecular Dynamics Simulation. In addition to the FT-IR and mid-IR pump—probe experiments, force field molecular dynamics (MD) simulations of these six solutions were performed: (i) 0.2 M NaN<sub>3</sub> + DMSO, (ii) 0.2 M NaN<sub>3</sub> + 2 M HIm + DMSO, (iii)

 $0.2 \text{ M NaN}_3 + 2 \text{ M } 1\text{-MeIm} + \text{DMSO}$ , (iv)  $0.2 \text{ M LiN}_3 + 2 \text{ M}$ HIm + DMSO, (v) 0.1 M  $Ca(N_3)_2 + 2$  M HIm + DMSO, and (vi) 0.1 M Mg( $N_3$ )<sub>2</sub> + 2 M HIm + DMSO. All simulations are carried out using the software package LAMMPS<sup>35,36</sup> and the OPLS-AA force field scheme.<sup>37</sup> Force field parameters of HIm are taken from the originally published OPLS-AA data set,<sup>3</sup> those of DMSO and 1-MeIm are taken from a later published addition,<sup>38</sup> cation parameters are used as in ref 39, and the azide ion is described as reported by refs 40-42. Data are collected from a 50 ns production run with a time step of 0.5 fs; the detailed simulation protocol is provided in the Supporting Information, and the detailed simulation protocol, simulation box sizes, and number of molecules of each species are provided in the Supporting Information. All trajectory analysis is performed by TRAVIS. 43,44 Radial distribution functions are plotted using the Python library Matplotlib, 36 while the spatial distribution functions are visualized by VMD<sup>45</sup> and Tachyon.<sup>46</sup>

A continuous debate is ongoing in the literature about the optimal choice of the force field for modeling the interaction between anions, cations, and solvent molecules. Probably the most accurate approach is specific parameter sets that are explicitly optimized for given target properties, followed by polarizable force fields, which are more generally applicable but computationally more expensive. This aspect is particularly relevant for ion pair formation of divalent cations in aqueous environments; see ref 16 and ref 47, where ion pairing might be overestimated. Here, we merely aim to obtain a qualitative comparison between different cations, and for the sake of easier reproducibility, we rely on the standard OPLS force field parametrization.

# 3. RESULTS AND DISCUSSION

3.1. FT-IR Absorption. We present the FT-IR spectra of the asymmetric stretching mode of sodium azide (NaN3) in DMSO (Figure 1, right panel, red solid line). The azide ion, N<sub>3</sub>, has three spectrally distinct vibrational modes: the symmetric stretching mode ( $v_1 = 1320 \text{ cm}^{-1}$ ), the asymmetric stretching mode ( $v_3 = 2000 \text{ cm}^{-1}$ ), and the degenerate bending mode ( $v_2 = 650 \text{ cm}^{-1}$ ). In the case of NaN<sub>3</sub>, we have identified two additional peaks at 1987 and 2023 cm<sup>-1</sup>, which are in Fermi resonance with the asymmetric stretching  $v_3$  state<sup>48</sup> and the contact ion pair of  $Na^+$  and  $N_3^-$ , respectively.<sup>11</sup> The Fermi resonance is shifted almost 17 cm<sup>-1</sup> from the position of  $(v_1 +$ v<sub>2</sub>) due to the thermal population of the bending state. The anharmonicity, the shift of the hot band relative to the fundamental band, was measured in the gas phase to be 14.1 cm<sup>-1</sup>. Figure 1(e),(f) also shows the asymmetric stretching mode of NaN3 in DMSO when HIm and 1-MeIm are added, respectively. The concentrations of HIm and 1-MeIm are varied from 0.5 to 2.0 M, while the concentration of NaN<sub>3</sub> has been kept at a fixed value of 0.2 M.

Figure 1(e) shows a decrease of intensity on the  $\nu_3$  band of the free azide ion when HIm is added to the solution. At first glance, the contact ion pair band at 2016 cm<sup>-1</sup> shows a red shift on top of an absorption increase following the rise in the HIm concentration. Alternatively, Figure 1(f) shows a negligible change of intensity on the  $\nu_3$  band of the free azide ion and contact ion pair bands when 1-MeIm is added to the solution. The intensity decrease of the  $\nu_3$  band of the free azide ion upon addition of HIm provides a clear signature of the direct interaction between azide and HIm molecules. In principle, the interaction of azide with HIm can show up as a

new vibrational transition located at a higher wavenumber. The intensity increments of the red-shifted NaN3 contact ion pair band may also show a spectral overlap with the new vibration band of the azide-HIm complex. To clarify this issue, we have performed experiments in two ways. First, we have taken the FT-IR spectra, as shown in Figure S3, of TBA-N3 in DMSO. TBA-N<sub>3</sub> does not form a contact ion pair in DMSO as the positively charged central nitrogen atom N<sup>+</sup> is surrounded and shielded by the long alkyl chains. The azide asymmetric stretching mode shows two vibrational features at 1987 and 2000 cm<sup>-1</sup>. After adding 2 M HIm with TBA-N<sub>3</sub> in DMSO, the FT-IR spectra show an additional peak at 2016 cm<sup>-1</sup>. Now it is clear that N<sub>3</sub> interacts with HIm through hydrogen bonding and gives an additional vibrational feature. Furthermore, we have taken another FT-IR spectra with  $Mg(N_3)_2$ in DMSO and they show three different vibrational features (Figure S4). The contact ion pair band of  $Mg(N_3)_2$  at 2057 cm<sup>-1</sup> is blue-shifted 57 cm<sup>-1</sup> from the solvent-separated N<sub>3</sub> band. In addition, with 2 M HIm with  $Mg(N_3)_2$  in DMSO, we have observed an additional peak at 2016 cm<sup>-1</sup> due to the interaction of N<sub>3</sub><sup>-</sup> with HIm. This observation even more clearly shows that solvent-separated N<sub>3</sub><sup>-</sup> and the contact ion pair N<sub>3</sub> both interact with HIm and the interaction of solventseparated N<sub>3</sub><sup>-</sup> with HIm gives an additional vibrational feature.

For further investigation, we performed a band profile analysis using a standard spectral deconvolution with pseudo-Voigt functions given by eq 1 over the whole range.

$$y = y_0 + A \left\{ \mu \left( \frac{2}{\pi} \right) \left( \frac{w}{4(x - xc)^2 + w^2} \right) + (1 - \mu) \right\}$$

$$\sqrt{\frac{4\ln(2)}{w\sqrt{\pi}}} \exp \left[ -\left( \frac{4\ln(2)(x - xc)^2}{w^2} \right) \right]$$
(1)

Here,  $y_0$  is an offset, A is the amplitude,  $\mu$  is the profile shape factor, w is the full width at half-maximum (fwhm), and xc is the line position. A detailed discussion of band profile analysis is discussed in Supporting Information Section 3 and the fwhm plot is given in Figure S2. The fwhm of the azide-HIm complex band at 2018 cm<sup>-1</sup> is broader than that of the free azide band, strongly suggesting the presence of hydrogen bonding.

For a detailed analysis of the interaction between NaN3 with HIm and 1-MeIm, we use 2D COS analysis. 49,50 The details of the 2D COS analysis are given in Supporting Information Section 7. As shown in Figures S5 and S6, we present the synchronous and asynchronous spectra of NaN<sub>3</sub> with (a) HIm and (b) 1-MeIm complexes, respectively. In the 2D map, we show the FT-IR spectra of these complexes from 1980 to 3500 cm<sup>-1</sup>. The azide asymmetric stretching mode is centered at 2000 cm<sup>-1</sup> and a broad vibration progression is visible from 2580 to 3500 cm<sup>-1</sup> due to the N-H stretching mode of HIm. The concentration-dependent synchronous spectrum (Figure S5(a)) exhibits an intense diagonal peak at 3137 cm<sup>-1</sup> and four auto peaks at 2000, 2017, 2838, and 2927 cm<sup>-1</sup>. Interestingly, the two bands at 2591 and 2689 cm<sup>-1</sup> do not generate any diagonal peak with azide asymmetric stretching modes. The off-diagonal peaks are also visible at (2800, 2000 to 3300, 2000) and (2820, 2016 to 3289, 2016) with two different signs. This is due to the decrease in the peak intensity at 2000 cm<sup>-1</sup>, coupled with the simultaneous increase in the peak intensity at 2016 cm<sup>-1</sup>. The sign of these two peaks in asynchronous spectra (Figure S5(a)) still remains same, which

means that the event at  $2000 \text{ cm}^{-1}$  occurs first compared to the event at  $2016 \text{ cm}^{-1}$ . Now, if we consider the synchronous spectra (Figure S5(b)) of 1-MeIm complexes with NaN<sub>3</sub>, the diagonal peaks are completely different compared to the case of HIm. If we observe carefully, the diagonal peak at 2017 cm<sup>-1</sup> is not there anymore, which signifies no interaction of the contact pair with 1-MeIm.

**3.2.** Estimation of Contact Pair Formation from MD Simulations. To get further insight into the abundance of the different azide ion pairs, we have performed molecular dynamics simulations. Radial and spatial distribution functions are computed from the simulation trajectories to assess and compare the preferred interactions of  $N_3^-$  in solutions of pure DMSO and with the addition of 2 M HIm or 1-MeIm. Figure 2(a) shows the radial distribution function (RDF) between

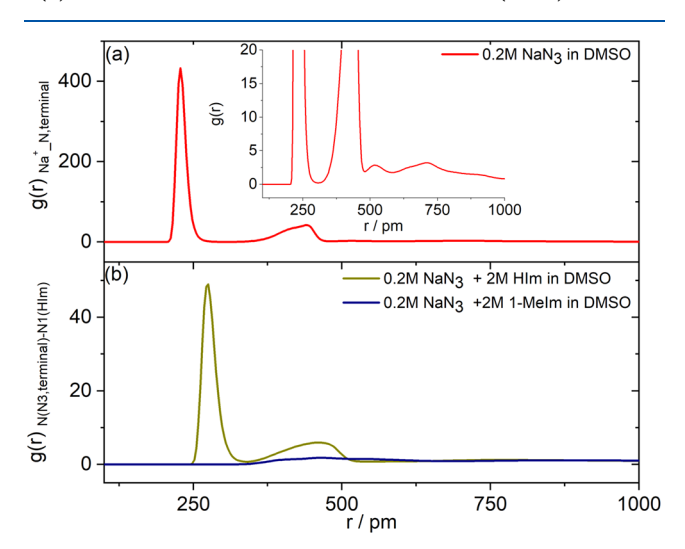


**Figure 2.** (a) Radial distribution function (RDF) between  $Na^+$  and the terminal N atoms in  $N_3^-$  in a solution of 0.2 M  $NaN_3$  in DMSO. There are two large peaks at 230 and 440 pm. The inset shows an enlarged view, visualizing smaller peaks at 520 and 710 pm. (b) RDF between terminal N atoms in  $N_3^-$  and the N1 atom in HIm (purple) and 1-MeIm (blue).

sodium cations and terminal azide N atoms obtained from an MD simulation of 0.2 M NaN $_3$  dissolved in DMSO. It represents the probability to find the terminal N atoms of N $_3$ <sup>-</sup> at a given distance "r" to the sodium cation. RDF values larger than 1 mean that the corresponding distance is more probable than for the case of uniform density. The first two peaks in the RDF have a high intensity value. With Na $^+$ -N distances of around 230 and 440 pm at their maxima, they correspond to sodium azide contact ion pairs. The two smaller peaks with maxima at around 520 and 710 pm represent the solvent-separated case, and at even larger distances, the RDF approaches unity. The large difference in the peak intensity indicates that the formation of sodium azide contact ion pairs is very dominant in DMSO.

The addition of 2 M 1-MeIm influences the Na-N RDF by increasing the intensity, whereas adding 2 M HIm decreases the intensity of the contact ion pair peaks, as shown in Figure S8(a). This effect can be quantified by calculating coordination numbers (CNs) as the integral of the first RDF peak according to eq 2

$$CN_{AB} = 4\pi \frac{N_{B}}{V_{\text{box}}} \int_{0}^{r_{\text{min}1}} r^{2} g(r)_{AB} dr$$
 (2)

where A is the reference species (here, Na<sup>+</sup>), B is the observed species (here, terminal N atoms of N<sub>3</sub><sup>-</sup>), and  $r_{\rm min1}$  is the distance coordinate of the first minimum. With CN<sub>NaN</sub> values of 0.882 in the solution containing 1-MeIm and 0.378 in the solution containing HIm, it becomes evident that sodium azide ion pairs occur more frequently in the solution of DMSO and 1-methylimidazole than in the solution of DMSO and imidazole. However, it has to be noted that Na<sup>+</sup>-N<sub>3</sub><sup>-</sup> ion pairs are still much more common than solvent-separated ions in the solution containing HIm.

As mentioned above, azide anions interact with imidazole but not with 1-methylimidazole where no hydrogen bond can be formed at the N1 atom of the 1-methylimidazole ring. The RDF between terminal azide N atoms and the N1 atom in imidazole or 1-methylimidazole (Figure 2(b)) confirms this finding. In the solution with 2 M HIm, the N–N RDF has a sharp first peak at 280 pm, the hydrogen bonding distance. The imidazole coordination number of azide (CN $_{\rm NN}$ ) has a value of 1.45, which indicates that this interaction has a high likelihood. A second smaller peak is observed below distances of 500 pm. In contrast, the RDF between terminal azide atoms and the N1 atom of 1-MeIm has no peak below distances of 300 pm and is also closer to a uniform density at larger distances, clearly showing that there is no preferential interaction between azide anions and 1-methylimidazole.

To identify whether azide aggregates are formed, we have taken the concentration-dependent FT-IR spectra of 5 mM to 0.5 M NaN<sub>3</sub> in DMSO. The FT-IR spectra are represented in Figure S9 and we do not observe any indication of aggregate formation. We have also computed the radial distribution function between the centers of mass of azide molecules in the solution containing 0.2 M NaN<sub>3</sub> and 2 M HIm (Figure S7). There is a considerable peak below 5 Å. From visual inspection of the simulation trajectory, we attribute this peak to some cases of two azide molecules sharing a sodium cation (azide-Na-azide). Aggregates of two sodium azide contact pairs are not observed.

So far, in our study, FT-IR absorption spectra, 2D correlation spectra, and MD simulations have revealed that azide anions form contact pairs with sodium cations in solutions of DMSO and their number is reduced to some extent upon addition of imidazole, which acts as an additional interaction partner.

To investigate whether sodium azide and azide-imidazole interactions are competitive, as illustrated in Figure 1(d), we computed spatial distribution functions (SDFs) of the terminal azide N atoms and the sodium cations around imidazole molecules. These are visualized as blue (N) and purple (Na<sup>+</sup>) isosurfaces in Figure 3. In agreement with our previous discussion, azide anions are located in the proximity of the N-H group of HIm. Sodium cations are in turn found in two distinct regions around the azide anions, indicating that  $N_3^$ ions can indeed interact simultaneously with both sodium cations and imidazole molecules. It remains, however, difficult to quantify how many of the N<sub>3</sub>-HIm interaction pairs are complemented by sodium cations to form the configuration Na+-N3--HIm. Interestingly, sodium also populates an additional region in proximity to the second imidazole ring N atom (N2), possibly due to the interaction with the free electron pair. This matches with the first peak at around 460 pm of the

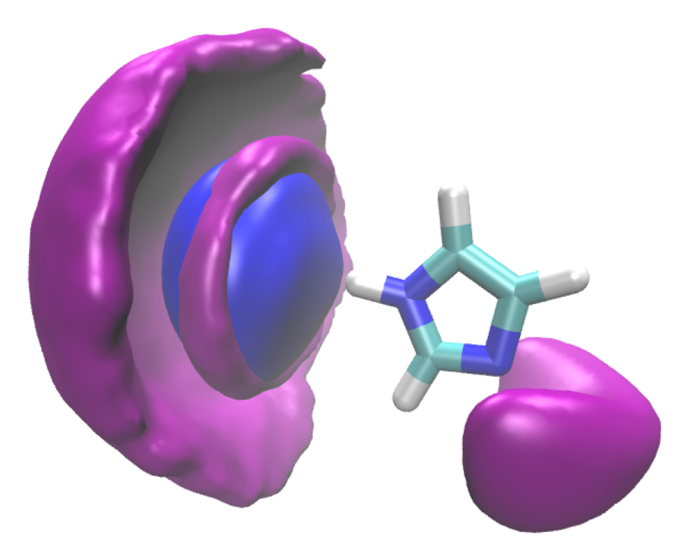


**Figure 3.** Spatial distribution functions (SDFs) of terminal azide N atoms (blue isosurface, visualized at an isovalue of  $1.65~\rm nm^{-3}$  out of  $55.192~\rm nm^{-3}$ ) and Na<sup>+</sup> (purple isosurface, visualized at an isovalue of  $0.34~\rm nm^{-3}$  out of  $11.1675~\rm nm^{-3}$ ) around HIm.

RDF between Na<sup>+</sup> and the N1 atom of HIm, which is provided in the Supporting Information (Figure S8(b)).

3.3. Mid-IR Transient Absorption Spectroscopy. 3.3.1. Azide Anion Interaction with HIm and 1-MeIm. Steady-state FT-IR measurements and molecular dynamics simulations clearly reveal that there is a strong interaction between  $N_3^-$  and HIm in the ground state. We performed mid-

IR pump—probe spectroscopy to investigate the interaction of azide with HIm and 1-MeIm in the vibrationally excited states. In mid-IR pump—probe spectroscopy, a strong pump pulse excites a molecular system from the  $\nu=0$  to the  $\nu=1$  state, and afterward, the relaxation of the state is monitored by the time-delayed probe. Transient pump—probe spectra in a spectral range from 1920 to 2080 cm<sup>-1</sup> are presented in the left panel of Figure 4 for (a) pure NaN<sub>3</sub>, (b) NaN<sub>3</sub> with HIm, and (c) NaN<sub>3</sub> with 1-MeIm in DMSO, showing the measured change  $\Delta A$  as a function of the probe frequency. For NaN<sub>3</sub> in DMSO (Figure 4(a)), the pump—probe signal displays an absorption decrease at around 2000–2045 cm<sup>-1</sup> and a redshifted positive absorption corresponding to the  $\nu=1$  to  $\nu=2$  transition at 1969 cm<sup>-1</sup>.

The absorption decreases on the  $\nu = 0$  to the  $\nu = 1$  state due to the contribution of ground-state bleach (GSB) and the stimulated emission (SE). The later  $\nu = 1$  to  $\nu = 2$  transition also gives rise to the red-shifted excited-state absorption (maximum peak at 1969 cm<sup>-1</sup>), which is overlapped with the ground-state bleach signal. When we add 2 M HIm with 0.2 M NaN3 in DMSO, we observe that the maximum peak of excited-state absorption (ESA) shifts to 1984 cm<sup>-1</sup>, as well a broadening of the spectral shape of the ESA. On the other hand, in the case of 0.2 M NaN<sub>3</sub> with 2 M 1-MeIm in DMSO, we do not observe a drastic change in the transient spectra compared to the case of 0.2 M NaN3 in DMSO. For a detailed analysis, we have taken the spectra at a 200 fs probe delay time from each system. Figure S10 shows that upon adding HIm, the peak at 1969 cm<sup>-1</sup> decreases, while the peak at 1985 cm<sup>-1</sup> increases, alongside spectral broadening. This suggests a

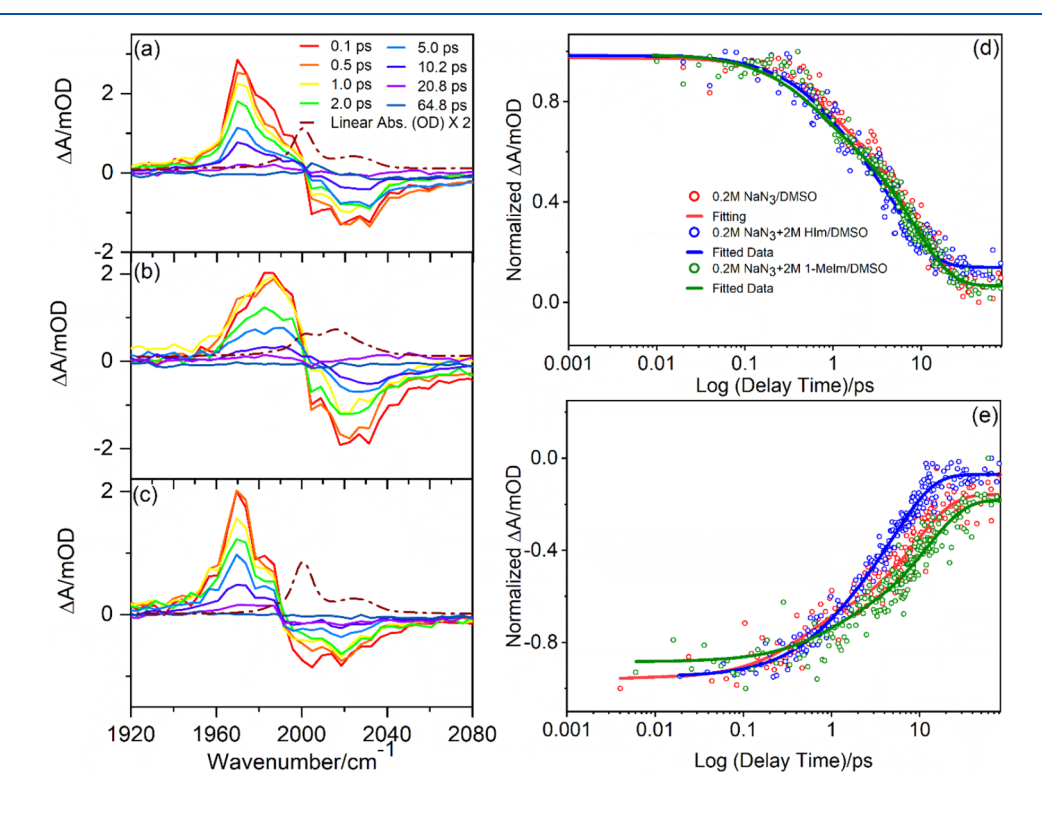


Figure 4. Left panel: transient mid-IR pump—probe spectra of (a)  $NaN_3$ , (b)  $NaN_3 + 2$  M HIm, and (c)  $NaN_3 + 2$  M 1-MeIm in DMSO after excitation with a mid-IR pulse centered at 2000 cm<sup>-1</sup>. The change in absorbance is plotted as a function of the probe frequency for the delay times given in the above panel. The wine dashed line shows the spectral range of the linear FT-IR absorption spectra of the azide stretching mode. Right panel: population kinetics at (d) 1969 and (e) 2015 cm<sup>-1</sup> of  $NaN_3$ ,  $NaN_3 + 2$  M HIm, and  $NaN_3 + 2$  M 1-MeIm in DMSO after excitation with 2000 cm<sup>-1</sup>. The open circles represent the experimental data, and the solid lines are the fitted curves.

Table 1. Biexponential Fitting Parameters of the Vibrational Population Decay of Free Azide Ions and Contact Ion Pairs in DMSO

sample name	freq (cm <sup>-1</sup> )	$t_1$ (ps)	$t_2$ (ps)	$A_1$ (%)	$A_2$ (%)	$Y_0$ (%)
0.2 M NaN <sub>3</sub> /DMSO	1970	$0.76 \pm 0.1$	$8.49 \pm 0.5$	$22.02 \pm 2.02\%$	$69.53 \pm 2.02\%$	$08.45 \pm 0.9\%$
0.2 M NaN <sub>3</sub> + 2.0 M HIm/DMSO	1983	$0.79 \pm 0.2$	$5.61 \pm 0.5$	$23.70 \pm 4.5\%$	$62.36 \pm 4.4\%$	$13.94 \pm 0.9\%$
0.2 M NaN <sub>3</sub> + 2.0 M 1-MeIm/DMSO	1966	$0.58 \pm 0.1$	$8.25 \pm 0.4$	$23.01 \pm 2.02\%$	$68.93 \pm 2.05\%$	$08.06 \pm 0.91\%$
0.2 M NaN <sub>3</sub> /DMSO	2015	$0.44 \pm 0.1$	$8.99 \pm 0.9$	$23.02 \pm 3.7\%$	$61.13 \pm 2.02\%$	$15.85 \pm 0.85\%$
0.2 M NaN <sub>3</sub> + 2.0M_HIm/DMSO	2015	$0.80 \pm 0.3$	$5.38 \pm 0.4$	$21.09 \pm 4.3\%$	$71.62 \pm 4.4\%$	$07.29 \pm 0.81\%$
$0.2 \text{ M NaN}_3 + 2.0 \text{ M } 1\text{- MeIm/DMSO}$	2015	$0.80 \pm 0.3$	$12.15 \pm 1.5$	$19.10 \pm 2.5\%$	$63.22 \pm 3.9\%$	$17.68 \pm 0.09\%$

hydrogen bonding interaction between NaN3 and HIm. Vibrational relaxation of the asymmetric stretching mode of the NaN<sub>3</sub> molecule in DMSO requires the initially excited mode to dissipate its energy to lower-frequency intramolecular vibrations and intermolecular modes, i.e., solvent bath modes. In general, the rate of the vibrational relaxation depends on the molecular coupling of the initially excited mode with the accepting modes.<sup>51</sup> The vibrational population decay of N<sub>3</sub> ions and contact ion pairs are displayed in Figure 4(d),(e). The changes in absorbance at two spectral regions in the ranges of the ESA and GSB are plotted as a function of pump-probe delay up to a delay time of 80 ps. The traces of  $\nu = 1$  to  $\nu = 2$ near the maximum of the peak for all three systems mentioned above show notable changes in their decay dynamics. Concomitantly, the decay kinetics of  $\nu = 0$  to  $\nu = 1$  near 2015 cm<sup>-1</sup> shows a major change in the presence of HIm and 1-MeIm. We have used a biexponential decay function to extract the decay time constants from the kinetic traces. The fitting parameters are summarized in Table 1. The first time constant  $(t_1)$  in the fitting parameters is due to the fast reorientation of azide. The second time constant  $(t_2)$  is longer and represents the vibrational relaxation time of the azide asymmetric stretching mode.<sup>26</sup> In both cases of different transitions from  $\nu = 0$  to  $\nu = 1$  and from  $\nu = 1$  to  $\nu = 2$ , the kinetic fitting results reveal faster dynamics in the addition of HIm with NaN3. In the presence of HIm, the azide anion dissipates energy to the accepting bath modes of the solvent and additionally to HIm, causing the faster dynamics. To support the assignment of  $t_1$  to the reorientation of azide, the vector autocorrelation of the azide anion was computed from a MD simulation of a solution containing 0.2 M NaN3 and 2 M HIm. The vector autocorrelation decay curve (Figure S11) is fitted with a bifunctional fit, yielding a fast time constant of 0.5

In presence of 1-MeIm, there is no chance of forming a hydrogen bond with an N<sub>3</sub><sup>-</sup> ion and hence we do not see a major change in the kinetics at 1966 cm<sup>-1</sup>. The GSB signal ( $\nu$ = 0 to v = 1 transition) shows a slower vibrational relaxation compared to the contact pair of NaN3, which is due to the presence of 1-MeIm with DMSO. The slowing of vibrational energy relaxation is caused by the decreasing of occupation numbers of bath modes that can accept the vibrational energy. In our simulation, we have already found more contact pairs of NaN<sub>3</sub> in the presence of 1-MeIm. The increment of contact pairs and the decrease of DMSO solvent bath mode are slowing down the vibrational relaxation process. A concentration-dependent study is carried out to get an overview of the systematic changes on the vibrational lifetime of azide in the presence of HIm and 1-MeIm, as discussed in the Supporting Information (Sections 12-16, as shown in Figures S12 and S13).

3.3.2. Effect of Different Counterions on the Azide-Hlm Interaction. In this section, we have focused on the impact of different counterions on the interaction of HIm on solventseparated and contact ion pair azides separately. The peak positions of the counterion pair azides are sensitively dependent on the size and charge of the counterion. For this reason, we have chosen different counterions, e.g., Li<sup>+</sup>, Ca<sup>2+</sup>, and Mg<sup>2+</sup>, which have different charges and sizes. Figure S14 represents the FT-IR spectra of azide stretching mode when different counterions are present. Similar to  $Na^+$  and  $Mg^{2+}$ , the azide ion also forms contact ion pairs with  $Li^+$  and  $Ca^{2+}$ . The contact ion pair vibration mode is significantly blue-shifted, and the shift is proportional to the polarizing power (P) of the counterion. This has been discussed earlier and the definition of the polarizing power is defined by Brooker and Berdig as follows:  $P = \frac{z}{rS_{\text{eff}}}$ , where  $S_{\text{eff}} = \frac{Sz^{1.27}}{I\sqrt{r}}$ , I is the ionization potential, z is the charge, and r is the radius of the counterion. We also performed a band profile analysis using a pseudo-Voigt function to extract the particular peak position and fwhm of the bands. Fitting parameters are tabulated in Table S6 and we observe that the fwhm of the contact ion pair peak is always larger than that of the solventseparated azide peak. The presence of counterions reduces the symmetry and varies the charge distribution of the azide asymmetric stretching mode. 11 Now, we have added 2 M HIm in each system where the counterions are different. Figure \$15 represents the FT-IR spectra of the asymmetric stretching mode of azide when different counterions and HIm are added. After the addition of HIm, the peak intensity of solventseparated azide goes down, and a new peak appears at 2016 cm<sup>-1</sup> in each case. The new peak is due to the contact pair complex of the N<sub>3</sub><sup>-</sup> ion with HIm. The intensity of the contact ion pair peaks also decreases slightly, except in the case of NaN<sub>3</sub>, where the effect is not visible due to the overlap of two different species. The contact ion pair peaks of  $Ca(N_3)_2$  and  $Mg(N_3)_2$  are slightly blue-shifted after adding HIm.

To understand the structures of different ion pairs of azide in the presence of HIm and different counterions, we performed MD simulations of the different solutions and computed the RDFs between the terminal N atoms of azide and the counterions. Intense azide-cation contact pair peaks are observed in all RDFs between the cations and terminal azide N atoms, which is shown in Figure S16 (a). The relative occurrence of the contact pairs measured by the coordination numbers (shown in Table S7) decreases in the order Na<sup>+</sup> > Li<sup>+</sup> > Mg<sup>2+</sup> > Ca<sup>2+</sup>. This gives an indication that the interaction between Ca<sup>2+</sup> and the azide anion is less preferable. On the other hand, azide-imidazole interactions are enhanced in the solutions containing divalent cations compared to the monovalent cations and decrease in the order Ca<sup>2+</sup>> Mg<sup>2+</sup>> Na<sup>+</sup> > Li<sup>+</sup>, which can be visible in Figure S16(B) and Table S7.

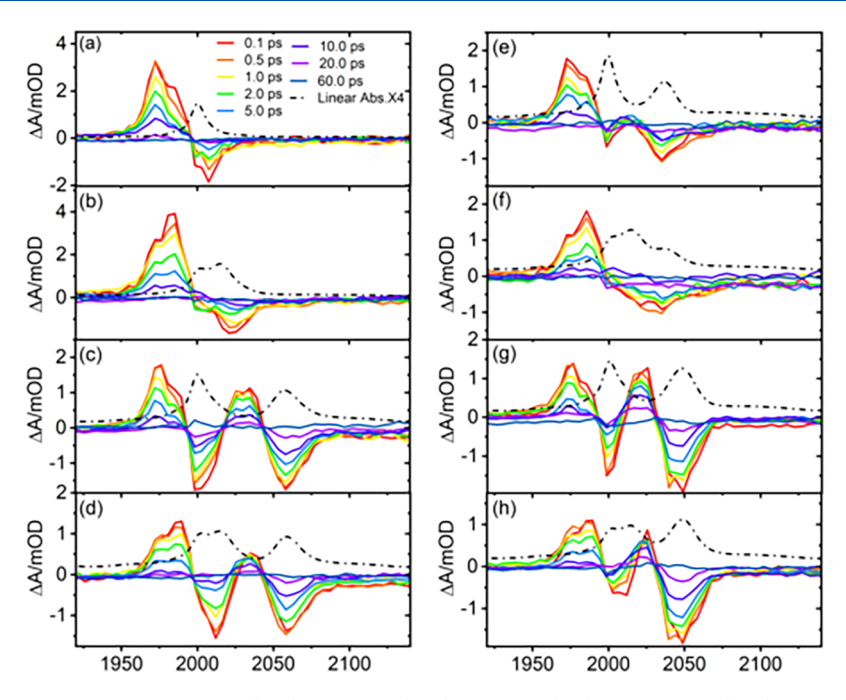


Figure 5. Transient mid-IR pump-probe spectra of (a, b) TBA-N<sub>3</sub>, (c, d) Mg-N<sub>3</sub>, (e, f) Li-N<sub>3</sub>, and (g, h)  $Ca-N_3$  with and without HIm in DMSO after excitation with 2000 cm<sup>-1</sup>. The change in absorbance is plotted as a function of the probe frequency for color-coded delay times. The black dashed line shows the linear absorption (OD) of the azide stretching mode.

There is a related computational study on the formation and stability of ion pairs (specifically, alkali and alkaline earth metal ions, dimethylphosphate cations, in aqueous solution, ref 16) where Mg<sup>2+</sup>-based ion pairs were found to be more stable than Ca<sup>2+</sup> cations, and Na<sup>+</sup> ions were found to form considerably weaker pairs. While a discussion of ion-specific trends in the stability of ion pair configurations is beyond the scope of the present work, we note that our observed ion ordering is not the same as reported in ref 16. A notable difference between this paper and our work is that the MD simulations reported in ref 16 were performed with water as the solvent, while our work here uses (water-free) DMSO, which makes it nontrivial to directly compare both settings. In our situation, the interplay of the salt ions and DMSO involves more complex geometrical constraints but also slower diffusion dynamics; hence, we believe that our simulations might simply not be fully converged in the statistical sense.

Figure 5 shows the transient IR pump-probe spectra of N<sub>3</sub> ions with different counterions and HIm. At first, we show the transient absorption spectra with pure TBA-N<sub>3</sub> in DMSO. As we have described in the earlier section, TBA-N3 does not form contact ion pairs in DMSO. The transient spectra show a bleach at 2000 cm<sup>-1</sup> and a red-shifted ESA at 1972 cm<sup>-1</sup>. We have added 2 M HIm with TBA-N<sub>3</sub> and observe an additional peak in the FT-IR spectra (Figure S4). Due to this additional peak, the bleach centered at 2021 cm<sup>-1</sup> becomes broader. The ESA absorption of TBA-N<sub>3</sub> with HIm shows that the peak intensity drops at 1972 cm<sup>-1</sup> and rises at 1983 cm<sup>-1</sup> compared to TBA-N<sub>3</sub> in DMSO. We now address the transient spectra of N<sub>3</sub><sup>-</sup> ions with (c) Mg<sup>2+</sup>, (e) Li<sup>+</sup>, and (g) Ca<sup>2+</sup> counterions. In all of the cases, we can easily distinguish two different contributions of the GSB signal due to the solvent-separated and contact ion pair azide ions. After adding HIm, we find a similar trend on the ESA, i.e., the peak intensity drops at 1972 cm<sup>-1</sup> and rises at 1983 cm<sup>-1</sup>, which can be clearly visible from panels (d), (f), and (h) in Figure 5. We have analyzed the data,

and the kinetic traces are fitted with a biexponential fitting function. In the case of Li+, after adding HIm, we have observed a broad bleach signal as the two contributions from the contact ion pair azide (LiN3) and the contact pair between an N<sub>3</sub><sup>-</sup> ion with HIm are at close spectral positions. For divalent atoms, (c) Mg<sup>2+</sup> and (g) Ca<sup>2+</sup>, we can identify two separate GSB signals from solvent-separated and contact ion pair azides in our transient spectra. From the kinetic analysis, as shown in Table S8, we have seen that the vibrational population relaxation times of free azide (solvent-separated) get 1.6-1.7 times faster with the addition of HIm. The vibrational population relaxation times of contact ion pair azide depend on the size and charge of the counterions in the presence of HIm. In the case of Li<sup>+</sup> and Mg<sup>2+</sup>, we have observed slightly faster vibrational population relaxation times in the presence of HIm. In contrast, the Ca<sup>2+</sup> contact ion pair azide shows an opposite trend (comparing the vibrational lifetimes at 2048 and 2050 cm<sup>-1</sup> listed in Table S7). From the MD simulation, we have understood that the interaction between Ca2+ and the azide anion is less preferable. The vibrational energy dissipation of azide to HIm and the solvent bath is greatly restricted by the Ca<sup>2+</sup> ion.

# 4. CONCLUSIONS

In a combined linear, ultrafast mid-IR pump—probe spectroscopy and ab initio molecular dynamics simulation approach, we study the ion pairing interactions between azide anions and HIm and 1-MeIm in DMSO. The azide ion forms contact ion pairs with alkali metal ions (Na<sup>+</sup> and Li<sup>+</sup>) as well as alkaline earth metal ions (Mg<sup>2+</sup> and Ca<sup>2+</sup>) in polar solvents with a high dielectric constant such as DMSO. The vibrational frequency of the azide ion in metal azide ion pairs exhibits a strong dependence on the counterions, allowing each metal azide pair to be spectrally differentiated from the free azide ion in the FT-IR spectrum. Additionally, these spectroscopic features are leveraged to investigate the vibrational population relaxation

dynamics of the individual free and metal azide ion pairs in DMSO solutions. In our present study, at first, we show that HIm can form a hydrogen bond with both the free azide  $(N_3^-)$ and contact ion pair azide (NaN3), while 1-MeIm cannot. We prove this by the change in linear FT-IR spectra, 2D COS analysis, and MD simulations. The vibrational lifetime of azide anions is measured in DMSO using mid-IR pump-probe transient absorption spectroscopy. Two different species of azide anions, solvent-separated and contact ion pairs, have been observed in the transient spectra. The vibrational lifetime of azide ions in metal azide ion pairs is longer than that of free azide ions and also depends on the charge and size of the counterions. In the presence of HIm, the vibrational energy dissipation from azide ions to HIm is more efficient than to DMSO molecules and accelerates the population relaxation of the azide ion. In our study, we have seen that the Ca<sup>2+</sup> ion is less favorable to interact with azide ions in comparison to Na<sup>+</sup>, Li<sup>+</sup>, and Mg<sup>2+</sup>. Our results exemplify the behavior of different counterions on the hydrogen bonding interaction of azide with HIm. We will further explore the impact of solvent fluctuations and spectral diffusion of these systems with two-dimensional infrared (2D-IR) spectroscopy. We anticipate that our ion pairing study would be very useful to study the process occurring in electrolyte solutions as well as in biological systems.

#### ASSOCIATED CONTENT

# **5** Supporting Information

The Supporting Information is available free of charge at https://pubs.acs.org/doi/10.1021/acs.jpcb.5c02025.

Mid-IR pump—probe experimental setup, force field classical molecular dynamics simulations, FT-IR spectra of the different complexes and the analysis of these, details of the 2D COS analysis, concentration-dependent transient absorption spectra of azide-HIm and 1-MeIm, and the radial distribution functions with different counterions (PDF)

#### AUTHOR INFORMATION

# **Corresponding Authors**

**Debkumar Rana** – Max Born Institut für Nichtlineare Optik und Kurzzeitspektroskopie, 12489 Berlin, Germany;

orcid.org/0000-0001-8165-3289;

Email: debkumar.rana@mbi-berlin.de

Daniel Sebastiani — Institut für Chemie, Martin-Luther-Universität Halle-Wittenberg, 06120 Halle (Saale), Germany; orcid.org/0000-0003-2240-3938; Email: daniel.sebastiani@chemie.uni-halle.de

Erik T. J. Nibbering — Max Born Institut für Nichtlineare Optik und Kurzzeitspektroskopie, 12489 Berlin, Germany; orcid.org/0000-0001-5874-8052; Email: erik.nibbering@mbi-berlin.de

#### Authors

Anna Luisa Upterworth – Institut für Chemie, Martin-Luther-Universität Halle-Wittenberg, 06120 Halle (Saale), Germany; orcid.org/0009-0003-0677-8745

Marc-Oliver Winghart — Max Born Institut für Nichtlineare Optik und Kurzzeitspektroskopie, 12489 Berlin, Germany; orcid.org/0009-0003-0213-4010

Complete contact information is available at: https://pubs.acs.org/10.1021/acs.jpcb.5c02025

#### Notes

The authors declare no competing financial interest.

### ACKNOWLEDGMENTS

The authors cordially acknowledge the financial support from the Deutsche Forschungsgemeinschaft (DFG) under Project 263266015 (project codes SE 1008/11-2 and NI 492/13-2) and the European Research Council (ERC) under the European Union's Horizon 2020 Research and Innovation Program (ERC Grant Agreement 788704). A.U. acknowledges funding by the DFG under the project code 436494874 (individual project A1).

#### REFERENCES

- (1) Marcus, Y. *Ions in Solution and Their Solvation*; John Wiley & Sons, Hoboken, New Jersey, United States, 2015.
- (2) Marcus, Y. Ionic Radii in Aqueous Solutions. *Chem. Rev.* **1988**, 88 (8), 1475–1498.
- (3) Baldwin, R. L. How Hofmeister Ion Interactions Affect Protein Stability. *Biophys. J.* **1996**, 71 (4), 2056–2063.
- (4) Lo Nostro, P.; Ninham, B. W. Hofmeister Phenomena: An Update on Ion Specificity in Biology. *Chem. Rev.* **2012**, *112* (4), 2286–2322.
- (5) Broering, J. M.; Bommarius, A. S. Evaluation of Hofmeister Effects on the Kinetic Stability of Proteins. *J. Phys. Chem. B* **2005**, *109* (43), 20612–20619.
- (6) Pinna, M. C.; Bauduin, P.; Touraud, D.; Monduzzi, M.; Ninham, B. W.; Kunz, W. Hofmeister Effects in Biology: Effect Of Choline Addition on The Salt-Induced Super Activity of Horseradish Peroxidase And Its Implication for Salt Resistance of Plants. *J. Phys. Chem. B* **2005**, *109* (34), 16511–16514.
- (7) Tomšič, M.; Bešter-Rogač, M.; Jamnik, A.; Neueder, R.; Barthel, J. Conductivity Of Magnesium Sulfate in Water from 5 to 35 C And from Infinite Dilution to Saturation. *J. Solution Chem.* **2002**, 31, 19–31
- (8) Wachter, W.; Fernandez, S.; Buchner, R.; Hefter, G. Ion Association And Hydration in Aqueous Solutions of LiCl And Li<sub>2</sub>SO<sub>4</sub> by Dielectric Spectroscopy. *J. Phys. Chem. B* **2007**, *111* (30), 9010–9017.
- (9) Kaatze, U.; Hushcha, T. O.; Eggers, F. Ultrasonic Broadband Spectrometry of Liquids A Research Tool in Pure And Applied Chemistry and Chemical Physics. *J. Solution Chem.* **2000**, 29, 299–
- (10) Eigen, M.; Eyring, E. M. Fast Protolytic Reactions in Aqueous Solutions of Aminobenzoic Acids. *J. Am. Chem. Soc.* **1962**, 84 (17), 3254–3256.
- (11) Le Borgne, C.; Illien, B.; Beignon, M.; Chabanel, M. Ion Association of Alkali And Alkaline Earth Metal Azides in Dimethylsulfoxide. Infrared Spectrometry And Ab Initio Calculations. *Phys. Chem. Chem. Phys.* **1999**, *1* (20), 4701–4706.
- (12) Marcus, Y.; Hefter, G. Ion Pairing. Chem. Rev. 2006, 106 (11), 4585–4621.
- (13) Park, K. H.; Choi, S. R.; Choi, J. H.; Park, S.; Cho, M. Real-Time Probing of Ion Pairing Dynamics with 2D-IR Spectroscopy. *Chem. Phys. Chem.* **2010**, *11* (17), 3632–3637.
- (14) Geissler, P. L.; Dellago, C.; Chandler, D. Kinetic Pathways of Ion Pair Dissociation in Water. *J. Phys. Chem. B* **1999**, *103* (18), 3706–3710.
- (15) Ghosh, D.; Sakpal, S. S.; Chatterjee, S.; Deshmukh, S. H.; Kwon, H.; Kim, Y. S.; Bagchi, S. Association—dissociation dynamics of ionic electrolytes in low dielectric medium. *J. Phys. Chem. B* **2022**, 126 (1), 239–248.
- (16) Fingerhut, B. P.; Schauss, J.; Kundu, A.; Elsaesser, T. Aqueous Contact Ion Pairs of Phosphate Groups with Na<sup>+</sup>, Ca<sup>2+</sup> and Mg<sup>2+</sup>– Structural Discrimination by Femtosecond Infrared Spectroscopy and Molecular Dynamics Simulations. *Z. Phys. Chem.* **2020**, 234 (7–9), 1453–1474.

- (17) Schauss, J.; Kundu, A.; Fingerhut, B. P.; Elsaesser, T. Contact ion pairs of phosphate groups in water: two-dimensional infrared spectroscopy of dimethyl phosphate and ab initio simulations. *J. Phys. Chem. Lett.* **2019**, *10* (20), 6281–6286.
- (18) Ohta, K.; Tominaga, K. Vibrational population relaxation of thiocyanate ion in polar solvents studied by ultrafast infrared spectroscopy. *Chem. Phys. Lett.* **2006**, 429 (1–3), 136–140.
- (19) Polak, M.; Gruebele, M.; Saykally, R. J. Velocity Modulation Laser Spectroscopy of Negative Ions. The n<sub>3</sub> Band of Azide Anion. *J. Am. Chem. Soc.* **1987**, *109* (10), 2884–2887.
- (20) Hamm, P.; Lim, M.; Hochstrasser, R. M. Non-Markovian Dynamics of The Vibrations of Ions in Water From Femtosecond Infrared Three-Pulse Photon Echoes. *Phys. Rev. Lett.* **1998**, *81* (24), No. 5326.
- (21) Owrutsky, J. C.; Raftery, D.; Hochstrasser, R. Vibrational Relaxation Dynamics in Solutions. *Annu. Rev. Phys. Chem.* **1994**, 45 (1), 519–555.
- (22) Zhong, Q.; Steinhurst, D.; Carpenter, E.; Owrutsky, J. Fourier Transform Infrared Spectroscopy of Azide Ion in Reverse Micelles. *Langmuir* **2002**, *18* (20), 7401–7408.
- (23) Zhong, Q.; Baronavski, A.; Owrutsky, J. Vibrational Energy Relaxation of Aqueous Azide Ion Confined in Reverse Micelles. *J. Chem. Phys.* **2003**, *118* (15), 7074–7080.
- (24) Lim, M.; Hamm, P.; Hochstrasser, R. M. Protein Fluctuations Are Sensed by Stimulated Infrared Echoes of The Vibrations of Carbon Monoxide And Azide Probes. *Proc. Natl. Acad. Sci. U.S.A.* 1998, 95 (26), 15315–15320.
- (25) Zhong, Q.; Owrutsky, J. Vibrational Energy Relaxation And Reorientation of Azide Ion Pairs in Dmso. *Chem. Phys. Lett.* **2004**, 383 (1–2), 176–180.
- (26) Son, H.; Kwon, Y.; Kim, J.; Park, S. Rotational Dynamics of Metal Azide Ion Pairs in Dimethylsulfoxide Solutions. *J. Phys. Chem. B* **2013**, *117* (9), 2748–2756.
- (27) Vamvouka, M.; Müller, W.; Ludwig, B.; Varotsis, C. Fourier Transform Infrared And Resonance Raman Studies of The Interaction of Azide with Cytochrome C Oxidase from Paracoccus Denitrificans. *J. Phys. Chem. B* **1999**, *103* (15), 3030–3034.
- (28) Cain, B. D.; Simoni, R. Proton Translocation by the F1FOATPase of *Escherichia coli*: Mutagenic Analysis of a Subunit. *J. Biol. Chem.* **1989**, 264 (6), 3292–3300.
- (29) Vik, S. B.; Antonio, B. J. A Mechanism of Proton Translocation By F1f0 Atp Synthases Suggested by Double Mutants of The A Subunit. *J. Biol. Chem.* **1994**, 269 (48), 30364–30369.
- (30) Kreuer, K.; Fuchs, A.; Ise, M.; Spaeth, M.; Maier, J. Imidazole And Pyrazole-Based Proton Conducting Polymers And Liquids. *Electrochim. Acta* **1998**, 43 (10–11), 1281–1288.
- (31) Shin, J. Y.; Wang, Y.-L.; Yamada, S. A.; Hung, S. T.; Fayer, M. D. Imidazole and 1-Methylimidazole Hydrogen Bonding and Nonhydrogen Bonding Liquid Dynamics: Ultrafast IR Experiments. *J. Phys. Chem. B* **2019**, 123 (9), 2094–2105.
- (32) Chakrabarty, S.; Barman, A.; Ghosh, A. Anomalous Infrared Absorbance of S= O: A Perturbation Study of  $\alpha$ -C-H/D. *J. Phys. Chem. B* **2022**, 126 (29), 5490–5496.
- (33) Chakrabarty, S.; Barman, A.; Ghosh, A. A disparity in solvatochromism of CO and SO vibrational probe: A study of structurally similar acetone and dimethyl sulfoxide. *J. Mol. Liq.* **2023**, 382, No. 122005.
- (34) Wei, Q.; Zhou, D.; Li, X.; Chen, Y.; Bian, H. Structural dynamics of dimethyl sulfoxide aqueous solutions investigated by ultrafast infrared spectroscopy: Using thiocyanate anion as a local vibrational probe. *J. Phys. Chem. B* **2018**, *122* (50), 12131–12138.
- (35) Plimpton, S. Fast Parallel Algorithms for Short-Range Molecular Dynamics. *J. Comput. Phys.* **1995**, *117* (1), 1–19.
- (36) Thompson, A. P.; Aktulga, H. M.; Berger, R.; Bolintineanu, D. S.; Brown, W. M.; Crozier, P. S.; in 't Veld, P. J.; Kohlmeyer, A.; Moore, S. G.; Nguyen, T. D.; et al. LAMMPS A Flexible Simulation Tool for Particle-Based Materials Modeling at The Atomic, Meso, And Continuum Scales. *Comput. Phys. Commun.* **2022**, 271, No. 108171.

- (37) Jorgensen, W. L.; Maxwell, D. S.; Tirado-Rives, J. Development and Testing of the OPLS All-Atom Force Field on Conformational Energetics and Properties of Organic Liquids. *J. Am. Chem. Soc.* **1996**, 118 (45), 11225–11236.
- (38) Jorgensen, W. L.; Ghahremanpour, M. M.; Saar, A.; Tirado-Rives, J. OPLS/2020 Force Field for Unsaturated Hydrocarbons, Alcohols, and Ethers. J. Phys. Chem. B 2024, 128 (1), 250–262.
- (39) Aqvist, J. Ion-Water Interaction Potentials Derived from Free Energy Perturbation Simulations. *J. Phys. Chem. A* **1990**, *94* (21), 8021–8024.
- (40) Olschewski, M.; Knop, S.; Lindner, J.; Vöhringer, P. Vibrational Relaxation of Azide Ions in Liquid-To-Supercritical Water. *J. Chem. Phys.* **2011**, 134 (21), No. 214504.
- (41) Morita, A.; Kato, S. Vibrational Relaxation of Azide Ion in Water: The Role of Intramolecular Charge Fluctuation And Solvent-Induced Vibrational Coupling. *J. Chem. Phys.* **1998**, *109* (13), 5511–5523.
- (42) Ferrario, M.; Klein, M. L.; McDonald, I. R. Dynamical Behavior of the Azide Ion in Protic Solvents. *Chem. Phys. Lett.* **1993**, 213 (5), 537–540.
- (43) Brehm, M.; Kirchner, B. TRAVIS—A Free Analyzer And Visualizer for Monte Carlo And Molecular Dynamics Trajectories. *J. Chem. Inf. Model.* **2011**, *51* (8), 2007–2023.
- (44) Brehm, M.; Thomas, M.; Gehrke, S.; Kirchner, B. TRAVIS-A Free Analyzer for Trajectories From Molecular Simulation. *J. Chem. Phys.* **2020**, *152* (16), No. 164105.
- (45) Humphrey, W.; Dalke, A.; Schulten, K. V. Visual Molecular Dynamics. J. Mol. Graph. 1996, 14, 33–38.
- (46) Stone, J. An Efficient Library for Parallel Ray Tracing and Animation, Masters Thesis; University of Missouri-Rolla, 1998.
- (47) Li, P.; Roberts, B. P.; Chakravorty, D. K.; Merz, K. M., Jr Rational design of particle mesh Ewald compatible Lennard-Jones parameters for + 2 metal cations in explicit solvent. *J. Chem. Theory Comput.* **2013**, 9 (6), 2733–2748.
- (48) Sando, G. M.; Dahl, K.; Owrutsky, J. C. Vibrational Spectroscopy And Dynamics of Azide Ion in Ionic Liquid And Dimethyl Sulfoxide Water Mixtures. *J. Phys. Chem. B* **2007**, *111* (18), 4901–4909.
- (49) Noda, I. Generalized Two-Dimensional Correlation Method Applicable to Infrared, Raman, And Other Types of Spectroscopy. *Appl. Spectrosc.* **1993**, *47* (9), 1329–1336.
- (50) Noda, I.; Ozaki, Y. Two-Dimensional Correlation Spectroscopy: Applications in Vibrational And Optical Spectroscopy; John Wiley & Sons: Hoboken, New Jersey, United States, 2005.
- (51) Oxtoby, D. W. Vibrational Relaxation in Liquids. Annu. Rev. Phys. Chem. 1981, 32 (1), 77–101.
- (52) Cartledge, G. Studies on the Periodic System. I. The Ionic Potential As A Periodic Function. *J. Am. Chem. Soc.* **1928**, *50* (11), 2855–2863.
- (53) Brooker, M. H.; Bredig, M. A. Significance of Both Polarizability And Polarizing Power of Cations in Nitrate Vibrational Spectra. *J. Chem. Phys.* **1973**, *58* (12), 5319–5321.